CONFIRMATION OF WIDE-FIELD SIGNATURES IN REDSHIFTED 21 CM POWER SPECTRA USING MURCHISON WIDEFIELD ARRAY OBSERVATIONS

Nithyanandan Thyagarajan[1*], Daniel C. Jacobs[1], Judd D. Bowman[1], N. Barry[2], A. P. Beardsley[2], G. Bernardi[3,4,5], F. Briggs[6,7], R. J. Cappallo[8], P. Carroll[2], A. A. Deshpande[9], A. de Oliveira-Costa[10], Joshua S. Dillon[10], A. Ewall-Wice[10], L. Feng[10], L. J. Greenhill[5], B. J. Hazelton[2], L. Hernquist[5], J. N. Hewitt[10], N. Hurley-Walker[11], M. Johnston-Hollitt[12], D. L. Kaplan[13], Han-Seek Kim[14,7], P. Kittiwisit[1], E. Lenc[15,7], J. Line[14,7], A. Loeb[5], C. J. Lonsdale[8], B. McKinley[14,7], S. R. McWhirter[8], D. A. Mitchell[16,7], M. F. Morales[2], E. Morgan[10], A. R. Neben[10], D. Oberoi[17], A. R. Offringa[6,7], S. M. Ord[11,7], Sourabh Paul[9], B. Pindor[14,7], J. C. Pober[2], T. Prabu[9], P. Procopio[14,7], J. Riding[14,7], N. Udaya Shankar[9], Shiv K. Sethi[9], K. S. Srivani[9], R. Subrahmanyan[9,7], I. S. Sullivan[2], M. Tegmark[10], S. J. Tingay[11,7], C. M. Trott[11,7], R. B. Wayth[11,7], R. L. Webster[14,7], A. Williams[11], C. L. Williams[10], J. S. B. Wyithe[14,7]

Draft version April 7, 2015

ABSTRACT

Here we confirm a recently predicted and previously unknown foreground signature in the 3D power spectra of high redshift 21 cm measurements, wherein the interferometer is sensitive to large-scale structure on all baselines. This is due to the inherently chromatic nature of a wide-field instrument response and is characterized by enhanced power from foreground emission in Fourier modes adjacent to those considered to be most sensitive to the cosmological H I signal. Thus it is a critical input to design and analysis choices of future instruments such as the Hydrogen Epoch of Reionization Array and the Square Kilometre Array. The simulation which predicted this feature was recently validated against Murchison Widefield Array data but this key element was at or below the noise level. In this paper, we improve the Murchison Widefield Array data sensitivity through coherent averaging of 12 independent snapshots aligned in local sidereal time across different observing nights, and provide the first confirmation of the prediction with a signal-noise ratio > 10.

Subject headings: cosmology: observations — dark ages, reionization, first stars — large-scale structure of universe — methods: statistical — radio continuum: galaxies — techniques: interferometric

1. INTRODUCTION

[1] Arizona State University, School of Earth and Space Exploration, Tempe, AZ 85287, USA
[2] University of Washington, Department of Physics, Seattle, WA 98195, USA
[3] Square Kilometre Array South Africa (SKA SA), Park Road, Pinelands 7405, South Africa
[4] Department of Physics and Electronics, Rhodes University, Grahamstown 6140, South Africa
[5] Harvard-Smithsonian Center for Astrophysics, Cambridge, MA 02138, USA
[6] Australian National University, Research School of Astronomy and Astrophysics, Canberra, ACT 2611, Australia
[7] ARC Centre of Excellence for All-sky Astrophysics (CAASTRO)
[8] MIT Haystack Observatory, Westford, MA 01886, USA
[9] Raman Research Institute, Bangalore 560080, India
[10] MIT Kavli Institute for Astrophysics and Space Research, Cambridge, MA 02139, USA
[11] International Centre for Radio Astronomy Research, Curtin University, Perth, WA 6845, Australia
[12] Victoria University of Wellington, School of Chemical & Physical Sciences, Wellington 6140, New Zealand
[13] University of Wisconsin–Milwaukee, Department of Physics, Milwaukee, WI 53201, USA
[14] The University of Melbourne, School of Physics, Parkville, VIC 3010, Australia
[15] The University of Sydney, Sydney Institute for Astronomy, School of Physics, NSW 2006, Australia
[16] CSIRO Astronomy and Space Science (CASS), PO Box 76, Epping, NSW 1710, Australia
[17] National Centre for Radio Astrophysics, Tata Institute for Fundamental Research, Pune 411007, India
[*] e-mail: t_nithyanandan@asu.edu

The epoch of reionization (EoR) commenced following the formation of the first stars and galaxies. It is characterized by a period of non-linear growth of matter density perturbations and astrophysical evolution in the Universe's history. Detection of redshifted 21 cm radiation of H I from this epoch is one of the most promising probes of the evolution of large scale structure characteristic of this epoch (Sunyaev & Zeldovich 1972; Scott & Rees 1990; Madau et al. 1997; Tozzi et al. 2000; Iliev et al. 2002).

While sensitive instruments such as the Square Kilometre Array (SKA) with the capability of direct imaging of redshifted H I become operational, numerous pathfinders and precursors such as the Murchison Widefield Array (MWA; Lonsdale et al. 2009; Tingay et al. 2013; Bowman et al. 2013), the Low Frequency Array (LOFAR; van Haarlem et al. 2013), the Precision Array for Probing the Epoch of Reionization (PAPER; Parsons et al. 2010), and the planned Hydrogen Epoch of Reionization Array[19] (HERA) have enough sensitivity for a statistical detection of the signal (Bowman et al. 2006; Parsons et al. 2012a; Beardsley et al. 2013; Dillon et al. 2013; Thyagarajan et al. 2013; Pober et al. 2014) and most of these are already operational.

The primary challenge to detection of cosmological H I from the EoR comes from continuum emission from Galactic and extragalactic foreground objects, relative to which the desired signal is $\sim 10^4$ times weaker (see, e.g.,

[19] http://reionization.org/

Di Matteo et al. 2002; Zaldarriaga et al. 2004; Furlanetto et al. 2006; Ali et al. 2008; Bernardi et al. 2009, 2010; Ghosh et al. 2012). Since the foregrounds and the signal have inherent differences in spatial isotropy and spectral smoothness (Morales & Hewitt 2004; Morales et al. 2006; Bowman et al. 2009; Liu & Tegmark 2011; Parsons et al. 2012b; Dillon et al. 2013; Pober et al. 2013), a detailed characterization of foreground emission has become essential (Bowman et al. 2009; Liu et al. 2009; Datta et al. 2010; Liu & Tegmark 2011; Morales et al. 2012; Trott et al. 2012; Pober et al. 2013; Dillon et al. 2014; Liu et al. 2014a,b; Thyagarajan et al. 2013, 2015).

A recent study by Thyagarajan et al. (2015) using instrument and all-sky foreground models has shed new light on the significant role played by the interplay between foreground emission and the nature of wide-field measurements, typical of most modern EoR experiments. It was noted to cause significant contamination in Fourier modes considered to be most sensitive for the cosmological H I signal. It has been shown that a careful design of antenna aperture can significantly mitigate this contamination. And an optimal weighting of foreground-contaminated Fourier modes may be required to extract the signal with maximum sensitivity. Thus, knowledge of such detailed foreground signatures becomes essential for design and analysis choices of future instruments such as HERA and SKA. This paper presents a follow-up analysis of that study. By using a larger volume of MWA data obtained independently over different nights pointed at the same region of sky, we confirm with high significance the presence of certain key characteristics (referred to as the *pitchfork* signature) of wide-field measurements predicted in the preceding study.

§2 is an overview of the role of wide-field measurements in the delay spectral domain and the predicted *pitchfork* signature. §3 describes the analysis of MWA data used to improve the dynamic range of the delay spectra. §4 describes the results and confirms the presence of the predicted wide-field effects. §5 summarizes our findings.

2. WIDE-FIELD EFFECTS IN DELAY SPECTRUM

Thyagarajan et al. (2015) have described in detail the effects of wide-field measurements as seen in the delay spectra of interferometer *visibilities*. Here, we list the relevant equations and give a brief overview of the wide-field signatures predicted therein.

The delay spectrum for a baseline vector, $\boldsymbol{b}$, is given by (Parsons et al. 2012a,b; Thyagarajan et al. 2013, 2015):

$$\tilde{V}_b(\tau) \equiv \int V_b(f) \, W(f) \, e^{i2\pi f\tau} \, df, \qquad (1)$$

with interferometer visibilities, $V_b(f)$, given by (van Cittert 1934; Zernike 1938; Thompson et al. 2001):

$$V_b(f) = \iint_{\text{sky}} A(\hat{\boldsymbol{s}}, f) \, I(\hat{\boldsymbol{s}}, f) \, W_{\text{i}}(f) \, e^{-i2\pi f \frac{\boldsymbol{b} \cdot \hat{\boldsymbol{s}}}{c}} \, d\Omega \qquad (2)$$

$$= \iint_{\text{sky}} \frac{A(\hat{\boldsymbol{s}}, f) \, I(\hat{\boldsymbol{s}}, f)}{\sqrt{1 - l^2 - m^2}} \, W_{\text{i}}(f) \, e^{-i2\pi f \frac{\boldsymbol{b} \cdot \hat{\boldsymbol{s}}}{c}} \, dl \, dm, \qquad (3)$$

where, $I(\hat{\boldsymbol{s}}, f)$ and $A(\hat{\boldsymbol{s}}, f)$ are the sky brightness and antenna's directional power pattern, respectively, as a function of frequency (f) and direction on the sky denoted

by the unit vector $\hat{\boldsymbol{s}} \equiv (l, m, n)$, $W_{\text{i}}(f)$ denotes instrumental bandpass weights, $W(f)$ is a spectral weighting function that controls the transfer function in the delay transform, $d\Omega = (1 - l^2 - m^2)^{-1/2} \, dl \, dm$ is the solid angle element to which $\hat{\boldsymbol{s}}$ is the unit normal vector, and c is the speed of light. $\tau = \boldsymbol{b} \cdot \hat{\boldsymbol{s}}/c$ is the geometric delay between antenna pairs measured relative to the zenith and provides a mapping to position on the sky.

The delay power spectrum is defined as:

$$P_{\text{d}}(\boldsymbol{k}_\perp, k_\parallel) \equiv |\tilde{V}_b(\tau)|^2 \left(\frac{A_{\text{e}}}{\lambda^2 \Delta B} \right) \left(\frac{D^2 \Delta D}{\Delta B} \right) \left(\frac{\lambda^2}{2k_{\text{B}}} \right)^2, \qquad (4)$$

with

$$\boldsymbol{k}_\perp \equiv \frac{2\pi(\frac{\boldsymbol{b}}{\lambda})}{D}, \qquad (5)$$

$$k_\parallel \equiv \frac{2\pi\tau \, f_{21} H_0 \, E(z)}{c(1 + z)^2}, \qquad (6)$$

where, A_{e} is the effective area of the antenna, ΔB is the bandwidth, λ is the wavelength of the band center, k_{B} is the Boltzmann constant, f_{21} is the rest frequency of the 21 cm radiation of H I, z is the redshift, $D \equiv D(z)$ is the transverse comoving distance, ΔD is the comoving depth along the line of sight, and h, H_0 and $E(z) \equiv [\Omega_{\text{M}}(1 + z)^3 + \Omega_{\text{k}}(1 + z)^2 + \Omega_\Lambda]^{1/2}$ are standard cosmology terms. In this paper, we use $\Omega_{\text{M}} = 0.27$, $\Omega_\Lambda = 0.73$, $\Omega_{\text{K}} = 1 - \Omega_{\text{M}} - \Omega_\Lambda$, and $H_0 = 100 \, \text{km s}^{-1} \, \text{Mpc}^{-1}$. $P_{\text{d}}(\boldsymbol{k}_\perp, k_\parallel)$ is in units of $\text{K}^2(\text{Mpc}/h)^3$.

In wide-field measurements, the steep rise in subtended solid angle near the horizon for a fixed delay bin size significantly enhances the integrated emission near the horizon delay limits. This is found to be true for diffuse emission even on wide antenna spacings because their foreshortening towards the horizon makes them sensitive to large angular scales that match the inverse of their foreshortened lengths. Typically, an antenna is most sensitive towards its primary field of view relative to the rest of the sky, which in conjunction with the aforementioned wide-field effects results in a characteristic *pitchfork* signature in the delay spectrum.

Detailed modeling presented in Thyagarajan et al. (2015) has shown this feature to be a leading source of contamination of the Fourier modes most sensitive to the EoR H I signal. And a dish-shaped antenna is found to yield the most desirable response from a foreground contamination viewpoint. Although there is marginal evidence for presence of this feature in the *zenith* snapshot used in their study, the high level of thermal noise prevented a robust confirmation. In this paper, we confirm the *pitchfork* signature using deeper data from the MWA.

3. THE MURCHISON WIDEFIELD ARRAY OBSERVATIONS

The MWA instrument configuration, EoR observations, and data analysis used in this study are already described in Thyagarajan et al. (2015) and references therein. In order to reduce thermal fluctuations while maintaining coherence, it is essential to average independent data sets obtained over the same region of sky with identical beamformer settings. Hence, we select a subset of MWA snapshots each of duration 112 seconds obtained

over different nights which are aligned to within 72 seconds of each other in *local sidereal time* (LST) around a mean LST of 0.04 hours with the MWA tile beam pointed at zenith. The database contains 14 snapshots satisfying these criteria. Two of these snapshots were found to contain amplitude and phase artifacts for a significant duration across different baselines. Hence, they have been excluded from our analysis.

The delay spectra of the rest of the snapshots were verified to be coherent in their amplitudes and phases. These complex valued delay spectra from independent snapshots are averaged together to lower thermal fluctuations without losing coherence from foreground contributions. The results are discussed below.

4. RESULTS

Figure 1 shows the delay spectra obtained from a single snapshot of MWA data (top), averaging LST aligned delay spectra from 12 individual snapshots from MWA observations on different nights (middle), and from modeling (Thyagarajan et al. 2015) with no thermal noise fluctuations (bottom), for reference. The dynamic range (in power spectrum units) in the averaged data (middle) is a factor $\gtrsim 10$ higher relative to that in a single snapshot (top) similar to the one used in Thyagarajan et al. (2015), and is consistent with the improvement expected from averaging 12 independent snapshots. With this improvement in sensitivity, the foreground power near the horizon limits (white dotted lines) has become $\gtrsim 10$ times more prominent. We now note that faint horizontal features appear at $\tau = \pm 0.78\,\mu s$ also as a result of lowering thermal fluctuations which is not seen in the single snapshot, thus confirming effective lowering of thermal fluctuations. We identify these faint features as the response in delay space of the MWA coarse band edges flagged periodically every 1.28 MHz.

Figure 2 shows the amplitudes of averaged delay spectra on three selected baseline vectors oriented northward. Data and noiseless models are shown in black and red respectively. The horizontal dotted black line denotes *rms* of thermal fluctuations estimated from data. The vertical dashed line denotes horizon delay limits, and the vertical dot-dashed lines denote delays at which the responses to coarse band edge flagging are expected.

The delay power spectra morphologies from data and modeling are remarkably similar despite some differences in the amplitude scales. We attribute these differences to uncertainties in the foreground model, the MWA tile power pattern, thermal fluctuations, and other uncertainties noted in Thyagarajan et al. (2015).

We focus on the peaks near the horizon limits in the data. Typically, the power near the negative horizon limit is seen with a signal-noise ratio (SNR) $\sim 10\text{-}100$, while that around the positive horizon limit is $\sim 100\text{-}1000$. The models of Thyagarajan et al. (2015) have noted that the foreground power near the horizon limits is due to the nature of wide-field measurements, and is predominantly composed of diffuse emission especially on baseline lengths $\lesssim 100$ m. Based on the morphological agreement between the data and the models, we conclude the features noted in our current analysis are a robust detection of the *pitchfork* signature predicted in Thyagarajan et al. (2015).
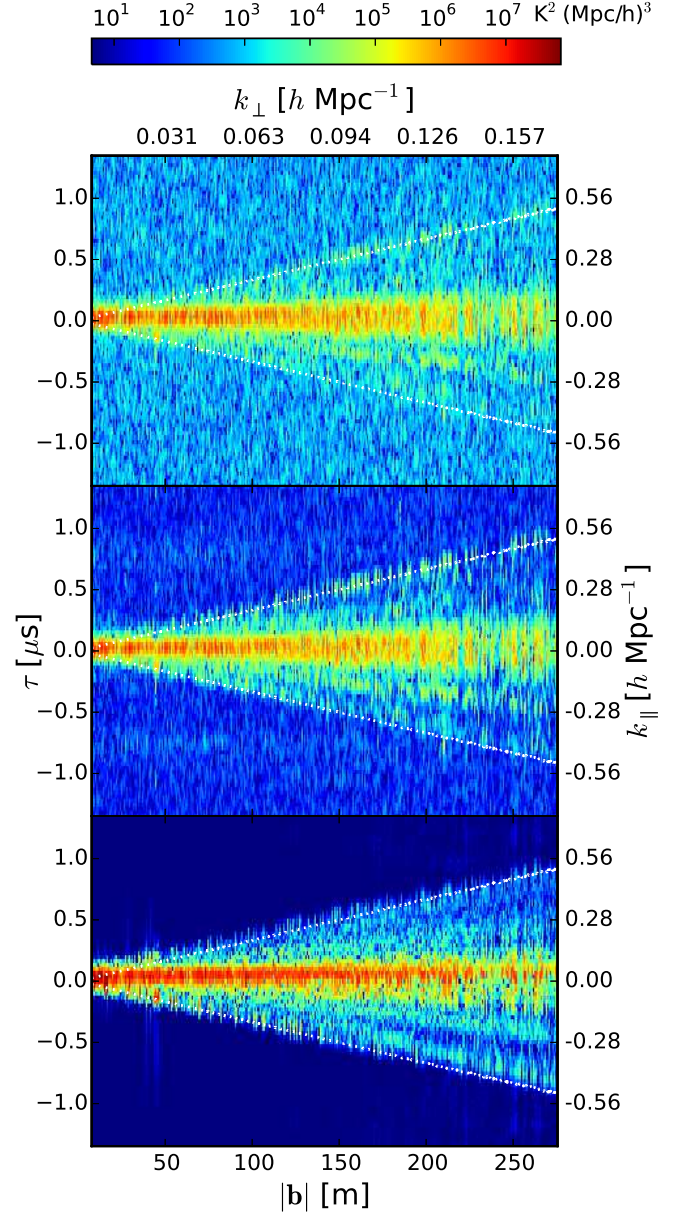

FIG. 1.— Delay power spectra obtained from a single snapshot (*top*), by averaging 12 snapshots of LST aligned MWA data (*middle*), and from modeling with no thermal noise added (*bottom*) shown for reference. The x-axis, denoted by $|\boldsymbol{b}|$ (and $k_\perp$), represents angular (and spatial) scales in the plane of the sky while the y-axis, shown in τ and $k_\parallel$, denotes the spatial scales along the line of sight. White dotted lines are the horizon delay limits. Dynamic range in the delay power spectra of MWA data has increased by a factor ~ 10 after averaging (middle) relative to that in a single snapshot (top). Power near the horizon limits caused by wide-field effects are prominent. Faint horizontal features at $\tau = \pm 0.78\,\mu s$ are visible due to effective lowering of thermal fluctuations and are the response to periodic coarse band edge flagging of MWA data every 1.28 MHz.

5. SUMMARY

Fluctuations of redshifted H I from the reionization epoch are extremely faint relative to the radio foregrounds. This poses perhaps the greatest challenge to
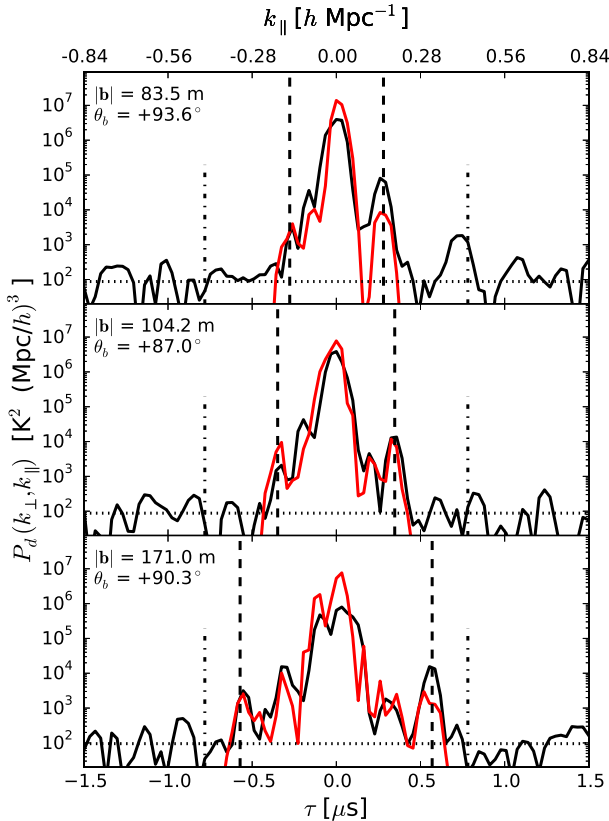
FIG. 2.— Delay power spectra on three antenna spacings oriented northward, obtained by coherent averaging of 12 snapshots aligned in LST. The averaged data and models are shown in black and red respectively. The antenna spacings are 83.5 m (*top*), 104.2 m (*middle*), and 171 m (*bottom*). The horizontal dotted line is the *rms* of thermal fluctuations. The vertical dashed lines denote the horizon delay limits. The vertical dot-dashed lines at $\tau = \pm 0.78\,\mu s$ correspond to grating responses of periodic flagging of bandpass at intervals of 1.28 MHz. The peaks close to the horizon delay limits are distinctly visible at $\sim$ 10-1000 σ levels. Differences between model and data are primarily attributed to uncertainties in the foreground model and the MWA tile power pattern.

geometric delays and subtended solid angles, besides an increase in sensitivity to larger scales caused by foreshortening of baseline lengths along these directions. Owing to its localization in the delay domain, it is a leading cause of contamination in Fourier modes most sensitive to the EoR H I signal.

Knowledge of these characteristics weigh heavily on choices in instrument design like antenna aperture and in data analysis such as optimal weighting schemes for future instruments such as HERA and SKA. We report the first robust detection of the *pitchfork* signature (which could not be confirmed earlier in single MWA snapshots due to large thermal fluctuations) with a signal-noise ratio > 10 made possible by coherent averaging of 12 independent LST-aligned snapshots from MWA observations.

EoR experiments and thus merits a detailed characterization in order to separate them from the desired cosmological H I signal.

In a recent study, through the use of all-sky foreground and instrument models, the role of wide-field nature of radio interferometric measurements, hitherto unpredicted, has emerged. Referred to as the *pitchfork* signature in the delay spectral domain, it is characterized by significant foreground power in the primary field of view and an enhancement in power near the horizon. The latter is due to the highly nonlinear mapping between

REFERENCES

Ali, S. S., Bharadwaj, S., & Chengalur, J. N. 2008, MNRAS, 385, 2166
Beardsley, A. P., Hazelton, B. J., Morales, M. F., et al. 2013, MNRAS, 429, L5
Bernardi, G., de Bruyn, A. G., Brentjens, M. A., et al. 2009, A&A, 500, 965
Bernardi, G., de Bruyn, A. G., Harker, G., et al. 2010, A&A, 522, A67
Bowman, J. D., Morales, M. F., & Hewitt, J. N. 2006, ApJ, 638, 20

—. 2009, ApJ, 695, 183
Bowman, J. D., Cairns, I., Kaplan, D. L., et al. 2013, PASA, 30, 31
Datta, A., Bowman, J. D., & Carilli, C. L. 2010, ApJ, 724, 526
Di Matteo, T., Perna, R., Abel, T., & Rees, M. J. 2002, ApJ, 564, 576
Dillon, J. S., Liu, A., & Tegmark, M. 2013, Phys. Rev. D, 87, 043005
Dillon, J. S., Liu, A., Williams, C. L., et al. 2014, Phys. Rev. D, 89, 023002

Furlanetto, S. R., Oh, S. P., & Briggs, F. H. 2006, Phys. Rep., 433, 181

Ghosh, A., Prasad, J., Bharadwaj, S., Ali, S. S., & Chengalur, J. N. 2012, MNRAS, 426, 3295

Iliev, I. T., Shapiro, P. R., Ferrara, A., & Martel, H. 2002, ApJ, 572, L123

Liu, A., Parsons, A. R., & Trott, C. M. 2014a, Phys. Rev. D, 90, 023018

—. 2014b, Phys. Rev. D, 90, 023019

Liu, A., & Tegmark, M. 2011, Phys. Rev. D, 83, 103006

Liu, A., Tegmark, M., Bowman, J., Hewitt, J., & Zaldarriaga, M. 2009, MNRAS, 398, 401

Lonsdale, C. J., Cappallo, R. J., Morales, M. F., et al. 2009, IEEE Proceedings, 97, 1497

Madau, P., Meiksin, A., & Rees, M. J. 1997, ApJ, 475, 429

Morales, M. F., Bowman, J. D., & Hewitt, J. N. 2006, ApJ, 648, 767

Morales, M. F., Hazelton, B., Sullivan, I., & Beardsley, A. 2012, ApJ, 752, 137

Morales, M. F., & Hewitt, J. 2004, ApJ, 615, 7

Parsons, A., Pober, J., McQuinn, M., Jacobs, D., & Aguirre, J. 2012a, ApJ, 753, 81

Parsons, A. R., Pober, J. C., Aguirre, J. E., et al. 2012b, ApJ, 756, 165

Parsons, A. R., Backer, D. C., Foster, G. S., et al. 2010, AJ, 139, 1468

Pober, J. C., Parsons, A. R., Aguirre, J. E., et al. 2013, ApJ, 768, L36

Pober, J. C., Liu, A., Dillon, J. S., et al. 2014, ApJ, 782, 66

Scott, D., & Rees, M. J. 1990, MNRAS, 247, 510

Sunyaev, R. A., & Zeldovich, Y. B. 1972, A&A, 20, 189

Thompson, A. R., Moran, J. M., & Swenson, Jr., G. W. 2001, Interferometry and Synthesis in Radio Astronomy, 2nd Edition (Wiley)

Thyagarajan, N., Udaya Shankar, N., Subrahmanyan, R., et al. 2013, ApJ, 776, 6

Thyagarajan, N., Jacobs, D. C., Bowman, J. D., et al. 2015, ArXiv e-prints, arXiv:1502.07596

Tingay, S. J., Goeke, R., Bowman, J. D., et al. 2013, PASA, 30, 7

Tozzi, P., Madau, P., Meiksin, A., & Rees, M. J. 2000, ApJ, 528, 597

Trott, C. M., Wayth, R. B., & Tingay, S. J. 2012, ApJ, 757, 101

van Cittert, P. H. 1934, Physica, 1, 201

van Haarlem, M. P., Wise, M. W., Gunst, A. W., et al. 2013, A&A, 556, A2

Zaldarriaga, M., Furlanetto, S. R., & Hernquist, L. 2004, ApJ, 608, 622

Zernike, F. 1938, Physica, 5, 785